

An automated salt-tracing gauge for flow-velocity measurement

Olivier Planchon,^{1*} Norbert Silvera,² Raphael Gimenez,³ David Favis-Mortlock,⁴ John Wainwright,⁵ Yves Le Bissonnais⁶ and Gerard Govers³

¹ IRD (Institut de Recherche pour le Développement), Laboratoire BioMCo, INRA-INAPG Bât. EGER, 78850 Thiverval-Grignon, France

² IRD (Institut de Recherche pour le Développement), BP 06 Vientiane, RDP Laos

³ Laboratory for Experimental Geomorphology, Redingenstraat 16, 3000 Leuven, Belgium

⁴ School of Geography, Queen's University Belfast, Belfast BT7 1NN, UK

⁵ Environmental Monitoring and Modelling Research Group, Department of Geography, King's College London, Strand, London WC2R 2LS, UK

⁶ INRA, Science du Sol, Avenue de la Pomme de Pin, BP 20 619, Ardon, 45166 Olivet cedex, France

*Correspondence to:

O. Planchon, Institut de

Recherche pour le

Développement (IRD),

Laboratoire BioMCo, INRA-

INAPG Bât. EGER, 78850

Thiverval-Grignon, France. E-mail:

oliver.planchon@grignon.inra.fr

Abstract

This article introduces the SVG (salt-velocity gauge), a novel automated technique for measuring flow velocity by means of salt tracing. SVG allows a high measuring rate (up to one every 2 seconds), short control section length (down to 10 cm), high accuracy (± 1.5 cm s⁻¹), and unbiased calculation of the mean velocity in experimental conditions with turbulent, supercritical flow.

A few cubic centimetres of saturated salt solution (NaCl) are injected into the flow at regular time intervals using a programmable solenoid valve. The tracer successively passes two conductivity probes placed a short distance downstream. The transformation of the signal between the two probes is modelled as a one-dimensional diffusion wave equation. Model calibration gives an estimation of the mean velocity and the diffusion for each salt plume.

Two implementations of the SVG technique are described. The first was an outdoors simulated rainfall experiment in Senegal (conductivity probes at 40 cm apart, 8 Hz measurement rate, salt injections at 10 second intervals). Mean velocity was estimated to range between 0.1 and 0.3 m s⁻¹. The second was a laboratory-based flume experiment (conductivity probes at 10 cm apart, 32 Hz, salt injections at 2 second intervals). Another SVG with probes at 34 cm apart was used for comparison. An acoustic Doppler velocimeter (ADV) was also used to give an independent assessment of velocity. Using the 10 cm salt gauge, estimated mean velocity ranged from 0.6 to 0.9 m s⁻¹ with a standard deviation of 1.5 cm s⁻¹. Comparisons between ADV, 10 cm SVG and 34 cm SVG were consistent and demonstrated that the salt-tracing results were unbiased and independent of distance between probes. Most peaks were modelled with $r^2 > 90$ per cent.

The SVG technology offers an alternative to the dye-tracing technique, which has been severely criticized in the literature because of the wide interval of recommended values for the correction factor α to be applied to the timings. This article demonstrates that a fixed value of α is inappropriate, since the correction factor varies with velocity, diffusion and the length of the control section. Copyright © 2005 John Wiley & Sons, Ltd.

Keywords: flow velocity; soil erosion salt; tracing

Received 29 October 2003

Revised 2 September 2004

Accepted 1 October 2004

Introduction

Measuring flow velocity in very shallow waters, with depths of centimetres or less, is a fundamental need in experimental studies of flow hydraulics, particularly those focusing on soil erosion by water. For example, the recent development of spatially explicit models of rill growth and initiation (see, e.g., Favis-Mortlock *et al.*, 2000) means

that corresponding spatially explicit measurements of flow velocity are needed for the thorough validation of such models.

To date, many technologies have been used for the estimation of flow velocities. Among these are hot film anemometry (Robinson and Cook, 1998; Ayala *et al.*, 2000), acoustic Doppler velocimetry (ADV) (Gimenez *et al.*, 2004), magnetic velocimeters and particle imaging velocimetry (PIV) (Adrian, 1991, Raffel *et al.*, 1998). However, these technologies have numerous limitations, in particular for field measurements of soil loss during rainfall: hot films are not suitable for measurements in flows carrying sediments because the thin layer of quartz which electrically insulates the platinum film can be abraded by sand particles or coated by colloidal deposits; ADV cannot measure flow paths of less than 1.5 cm in depth and 8 cm in width; magnetic velocimeters need streams even deeper; and PIV, because it involves sophisticated equipment such as laser planes and high-speed digital cameras, is dedicated to laboratory experiments and measurement in artificial channels (Liu *et al.*, 2001). Commonly, dye tracing or salt tracing is the only available solution.

There is also a more fundamental problem. Both dye and salt tracing involve following a tracer plume by eye or electronically in order to calculate V_{\max} , the velocity of the leading edge of the plume. A correction factor α is then applied to convert V_{\max} into V_{mean} , the mean flow velocity ($V_{\text{mean}} = Q/A$ where Q is the discharge and A the cross-sectional area of flow).

Horton *et al.* (1934) proposed $\alpha = 0.67$, which assumes the theoretical case of infinitely wide, perfectly laminar flow on a smooth and immobile bed. However the value of α was subsequently found to depend on a range of parameters including Reynolds number Re (Emmett, 1970; Li *et al.*, 1996), gradient (Li *et al.*, 1996; Li and Abrahams, 1997), sediment load (Li and Abrahams, 1997) and even experimental details such as the quantity of dye and the length of the control section (Takken, 2000). The result of these investigations has been a steady widening of the range of observed α (generally $0.2 < \alpha < 0.8$, with some exceptions reported outside this interval). This situation is carefully reviewed by Dunkerley (2001) based on a major compilation of dye and salt-tracing results, either derived from the literature (for $200 < Re < 14\,000$, i.e. from very laminar to very turbulent flows), or from his own experiments on laminar flows ($100 < Re < 500$). Additionally, he reported that not only Re , but also the size of protruding roughness elements, affects α values. Myers (2002) later demonstrated from fluid-flow principles that α cannot be constant in laminar flows. Dunkerley concluded pessimistically regarding the usefulness of dye and salt tracing for evaluating V_{mean} . He subsequently proposed a simple technology to measure specifically the surface flow velocity. It is based on the use of a small floating reflector target (a piece of ordinary aluminium foil) that is carried on the surface tension film, and which passes between two reflective sensors mounted above the flow (Dunkerley, 2003). Results show that, in laminar flow, the float moved at the same velocity as the leading edge of a dye plume. His technology therefore provides an improved alternative to dye timing for measuring V_{\max} , but still fails to evaluate V_{mean} without knowing α .

In this article, a new technology is presented for measuring the mean velocity of the salt plume, denoted V_{salt} . It consists of injecting a salt plume into the flow and recording the flow conductivity at two sections downstream. A one-dimensional diffusion model is adjusted to fit the transformation of the upstream peak into the downstream peak. The model has two coefficients; one is V_{salt} and the other is D , the diffusion coefficient of the model. Note that the word 'diffusion' as used here specifically reflects and results from the use of a diffusion equation. It aims to catch in a single black box value the complex behaviour of the salt, which in turns results from the combination of true diffusion, eddy mixing and lateral and vertical variations of flow velocity. Note too that V_{salt} is not necessarily V_{mean} since the salt concentration may not be uniform in the flow. Comparisons between V_{salt} and V_{mean} have been carried out: results are discussed near the end of this paper.

Material and methods

General

The salt-velocity gauge (SVG) measuring technique described in this paper is not a 'closed' technology, in that it may readily be modified for specific situations. Thus this section first outlines elements that are likely to be common to all applications, while the following two sections describe details that are specific to the two implementations which form the focus of the last part of this paper.

The SVG essentially consists of a solenoid valve injecting a saturated solution of domestic salt (NaCl) into the flow, and two conductivity probes, which measure the apparent conductivity downstream. A datalogger (such as the Campbell CR10x used in both studies described here) both controls the valve and takes the measurements. The datalogger's built-in half-bridge method is used for conductivity measurements: Figure 1 shows the connection diagram. Measurements are replicated at the two probe terminals, one of which has a +2.5 V excitation with the other having a -2.5 V

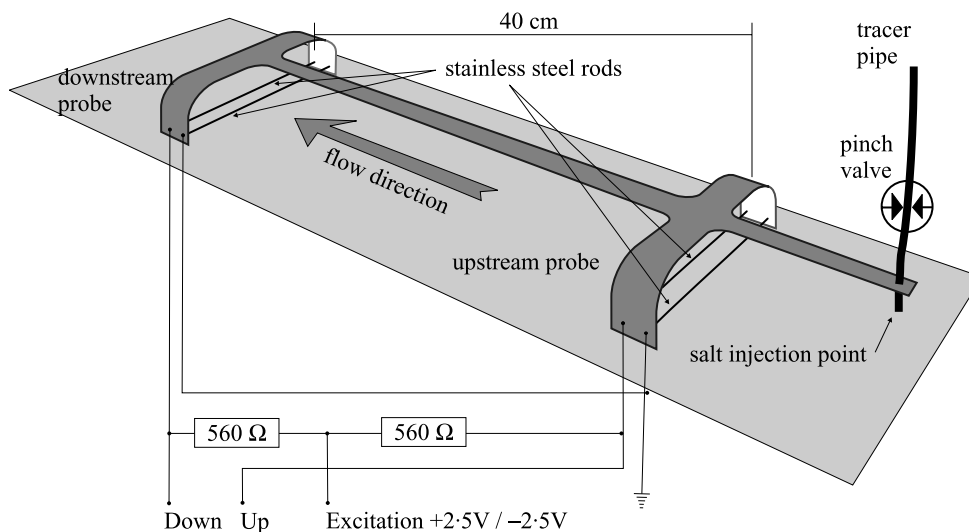


Figure 1. The salt-tracing velocimeter. Version with horizontal probes as used in the interrill experiment.

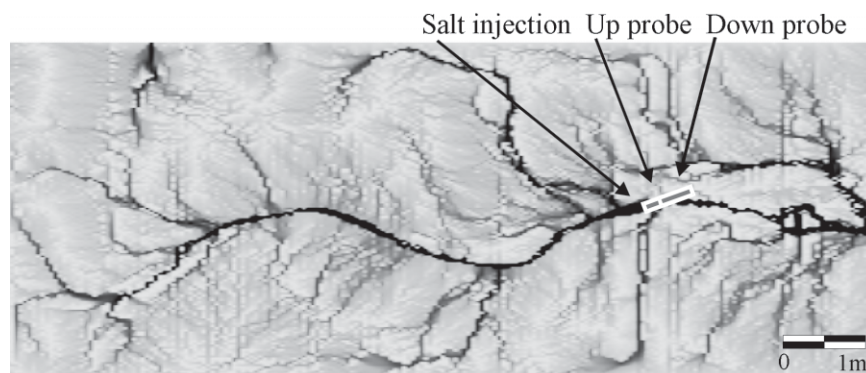


Figure 2. Rainfall simulation plot used in the inter-rill experiment at Thies, Senegal. Map of estimated flow rates and probe location.

excitation. This arrangement avoids probe polarization. The final result is calculated as the ratio ρ between measurement and excitation voltages, which ranges between 0 (short circuit) and 1 (open circuit). Assuming a linear response of the probes, salt concentration C is proportional to $(1/\rho - 1)$. The value $(1/\rho - 1)$ is called 'relative salt concentration' hereafter.

When dedicated to a single SVG, a datalogger such as the CR10x can run at 32 Hz. However, although conductivity measurements are logged as occurring at the same time, the serial nature of the datalogger means that processing of the measurements taken at the two probes is actually not simultaneous. There is a lag (here 4.4 ms): this must be taken into account, and is done so here at the end of the post-processing calculations. Note also that when multiple SVGs are connected to the same CR10x, the measurement frequency must be lowered to 16 Hz (for up to 2 SVGs) or even to 8 Hz (for more than 2 SVGs); however, the time lag between the measurement of the two probes of a given salt-gauge remains 4.4 ms in all cases.

The inter-rill test

A first experiment was carried out with the IRD (Institut de Recherche pour le Développement) large rainfall simulator (Planchon *et al.*, 2000a), on sandy soil in Thies, Senegal. An outdoor experimental plot was used, which was 10 m long, 4 m wide, and with a 1 per cent mean slope. Figure 1 illustrates the velocity probe used. It consists of two conductivity probes, placed 40 cm apart, each constructed of two horizontal stainless steel rods. A solenoid valve was opened at 10 second intervals for one second, releasing about 3 ml of salt solution at a time. Figure 2 shows the device location and the flow paths as calculated using the flow-accumulation algorithm of Quinn *et al.* (1991), using

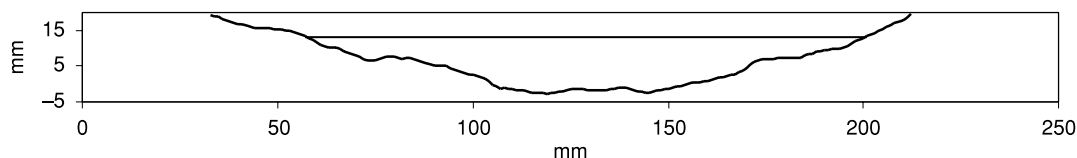


Figure 3. Cross section of the experimental rill.

microtopography data obtained after one hour of rainfall by the reliefmeter of Planchon *et al.* (2000b); grid spacing was 2.5 cm across the plot and 5 cm longitudinally. Rainfall intensity was held constant, at 75 mm h⁻¹. Salt tracing was recorded in the main flow concentration during the first 15 minutes of run-off.

The rill-flow test

A second experiment was part of the flume study carried out by Gimenez *et al.* (2004) in the experimental geomorphology laboratory of the Katholieke Universiteit Leuven. The flume (2.5 m long and 40 cm wide, with 8.75 per cent slope) was filled with loamy soil sieved at 2 cm. A rill was preformed in the flume bed after seven runs of 1 minute each at a discharge of 1 l s⁻¹. The flume surface was then fixed by spraying over the entire surface a 1:5 dilution of polyester resin and acetone. Acetone dilution thinned the resin so that it could infiltrate the soil one or two centimetres deep, resulting in a strong crust after it dried. On the other hand, spray application ensured that all the resin infiltrated the soil and thus preserved the original bed roughness very closely. The production of large quantities of acetone fumes is the only concern about this technique: safety rules must be strictly observed.

Velocities measured in the fixed rill using dye tracer were compared with those measured in the rill just before the polyester resin was created. Values obtained were 0.45 m s⁻¹ and 0.48 m s⁻¹ before and after the fixing of the rill bed, respectively. The similarity of these results suggests that the fixation of the bed did not significantly affect its roughness.

The rill showed a succession of steps and pools separated by headcuts, resulting in complex hydraulics within the step–pool system. The longest step was long enough to have the water surface parallel to the rill bed for a longitudinal distance of 20 cm. This section was chosen as the control section for ADV comparison. In this control section, the flow was shallow (depth 14 to 19 mm), turbulent ($Re = 9000$) and supercritical ($Fr = 1.4$). Figure 3 shows a cross section. ADV measurements were made at every centimetre in the control section, both at the water surface and at the bottom; samples were taken at 5 Hz and averaged over 20 seconds.

An SVG was specially designed for this study (Figure 4), and differed from that used in the first experiment (see also the discussion section later in this paper). The conductivity probes for this version of the device consist of four vertical stainless steel pins arranged at 1 cm intervals. All odd and all even pins are connected together, giving two groups, each of which forms one probe terminal; thus each probe works as two pairs of electrodes in parallel. This offers at the same time a large measuring width and a reasonable sensitivity.

Salt injection lasted 0.25 s and was repeated every 2 s for 3 minutes, yielding 90 velocity measurements at each location. Salt-tracing velocities were taken at 5 cm intervals along the flume, resulting in a set of 38 locations, five of which were located in the control section.

Continuous equations and numerical solution

The flow velocity within the plume can be conceptualized as a mean velocity V_{Salt} perturbed by various diffusion-inducing processes, including molecular diffusion, eddy mixing, velocity gradients in the flow, etc. Because only the value of V_{Salt} is of interest, and not the details of the diffusive processes, and also because of a lack of data to build a more refined model, it is proposed that all of these processes can be lumped into a single, one-dimensional, diffusion parameter. This approach leads to the use of Equation 1, which is the diffusion wave equation in one dimension.

$$\frac{\partial C}{\partial t} = -V_{\text{Salt}} \frac{\partial C}{\partial x} + D \frac{\partial^2 C}{\partial x^2} \quad (1)$$

where C is the relative salt concentration (g l⁻¹), t is time (s), V_{Salt} is the mean flow velocity within the salt plume (m s⁻¹) and D is the diffusion coefficient (m² s⁻¹).

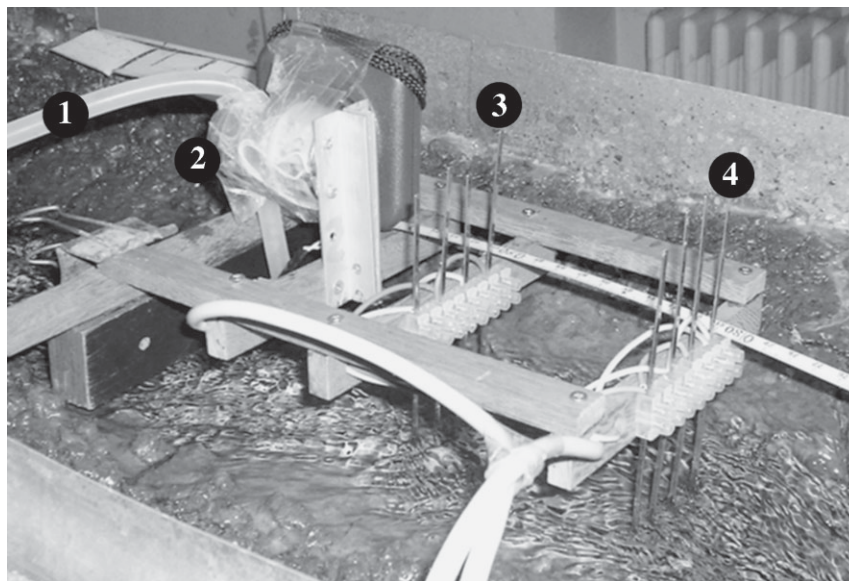


Figure 4. The 10 cm salt gauge used in the rill study. Salinity probes are spaced 10 cm from each other. Salt injection was 7 cm upstream of the first probe. 1: salt pipe. 2: pinch valve. 3: upstream probe. 4: downstream probe.

Hayami (1951), reported by Henderson (1966), solved Equation 1 analytically when the concentration at distance $x = 0$ is a Dirac function, i.e. a unit peak injected at $x = 0$ and $t = 0$ in infinitely small space and time. Equation 2 shows Hayami's solution (notation is detailed at the end of the article).

$$C(x, t) = \frac{x}{2\sqrt{\pi Dt^3}} \exp\left(\frac{-(V_{\text{Salt}}t - x)^2}{4Dt}\right) \quad (2)$$

where $C(x, t)$ is Hayami's solution of Equation 1 (g l^{-1}) at time t and distance x from injection.

While Hayami's work was aimed at modelling much larger flows, those of river floods, there is no *a priori* reason why it is not applicable in our smaller-scale case. In the experiments reported here, the first probe is at $x = 0$ and the second probe is at $x = d$. The initial condition at $x = 0$ is not a Dirac function but $C_1(t)$, the observed relative salt concentration at the first probe (probe 1). In this case, the solution of Equation 1 at $x = d$ is the convolution of $C_1(t)$ and $C(d, t)$, as expressed in Equation 3.

$$C_2(t) = \int_0^{\infty} C_1(t - u)C(d, u) du \quad (3)$$

where $C_2(t)$ is the relative salt concentration at the second probe.

The approach taken requires the optimization of V_{Salt} and D in order to fit the modelled values of $C_2(t)$ to the observed ones. Optimizing V_{Salt} was difficult when the signal quality was poor. For this reason the time to peak concentration t_p is optimized instead. V_{Salt} is subsequently calculated from t_p and D using Equation 4.

$$V_{\text{Salt}} = \frac{\sqrt{d^2 - 6Dt_p}}{t_p} \quad (4)$$

The convolution represented by the integral in Equation 3 is calculated with the function *convlv* of Press *et al.* (1992), which involves fast Fourier transforms (FFTs). Optimization is carried out with the conjugate gradient method (Acton, 1970) implemented by Press *et al.* (1992) (function *powel*). A 1.7 GHz PC can model 20 peaks per second with this method, allowing hours of conductivity records to be transformed into velocities within minutes.

Implementation

The model implementation needs three main steps to transform the raw measured signal into a time series of velocity.

1. Sequentially extracting all pairs of peaks
2. Obtaining the best approximation of the parameters to calibrate
3. Calibration of the model itself.

Splitting the input signals into pairs of peaks

Splitting any periodic signal into single periods is straightforward when the frequency is known, the signal is not noisy and periods are regularly spaced. It is much more difficult however when the signal quality is poor (due to electronic noise, an unsteady base line, irregularities of peaks heights, missing peaks etc.). Poor signal quality can often be the case with salt tracing. A robust method based on the comparison of two different smoothings of the signal was developed. Savitsky-Golay smoothing filters are used (function *avgol*, Press *et al.*, 1992): these filters are a generalization of the moving average technique where the function that is fitted in the moving window is not restricted to the average (i.e. the polynomial of degree zero) but may be a polynomial of any order. A given point of the window, usually the centre, is then set to the value of that polynomial.

The first smoothing used a third-degree polynomial and a window width of $N/2$, where N is the average number of data points between two peaks. N equals the time lag between two peaks (in seconds) over the datalogger sampling frequency (in Hz). This first smoothing drastically smoothed the peaks, but preserved their general shape. The second smoothing used a moving average, and a window width of $2N$. This approach removed the peaks and gave the mean signal height. The difference between the two adjustments is a smooth line alternately positive and negative. The maximum of each positive segment is a peak top, and the minimum of each negative segment separates two peaks.

After the signals from the two probes have been processed in this way, each peak from the first probe is associated with the relevant peak from the second probe and the pair is sent to the optimization process.

Obtaining a first approximation of parameters

Experience has shown that special attention must be paid to the choice of a good initial value for peak time t_p otherwise optimization fails. The method used is the function *correl* of Press *et al.* (1992). Given two sampled signals g and h , function *correl* returns the correlation Corr defined by

$$\text{Corr}(g, h)_i = \sum_{k=0}^{N-1} g_{k+i} h_k \quad (5)$$

where N is the common length of sequence of values of g and h .

If g and h are two periodic signals of the same frequency with a phase shift of n sampled data then $\text{Corr}(g, h)_n$ will be a maximum. Correlating the two sampled peaks this way gives a reliable estimate of their time lag.

D is initialized to a low value, $0.001 \text{ m}^2 \text{ s}^{-1}$, as the optimization procedure withstands poor initial values of D .

The third step is the calibration itself, which is a simple call to function *powel*. The model quality is estimated by the correlation coefficient between the observed peak at the downstream probe and the calibrated one.

Results

Modelling peaks

Figure 5(a) shows a series of peaks modelled in the inter-rill (field) experiment, with a velocity of $0.15\text{--}0.2 \text{ m s}^{-1}$. Fig. 5b is from the rill-flow (laboratory) experiment, with a velocity of 0.6 m s^{-1} . These figures show an excellent fit of the model to the data, and indeed 75 per cent of all peaks collected have been modelled with $r^2 \geq 0.9$.

Variability of measurements

The rill-flow case In the rill experiment, discharge was held constant. Thus, assuming no uncontrolled variations in discharge, the standard deviation of velocity represents the overall accuracy of the measuring process: this includes

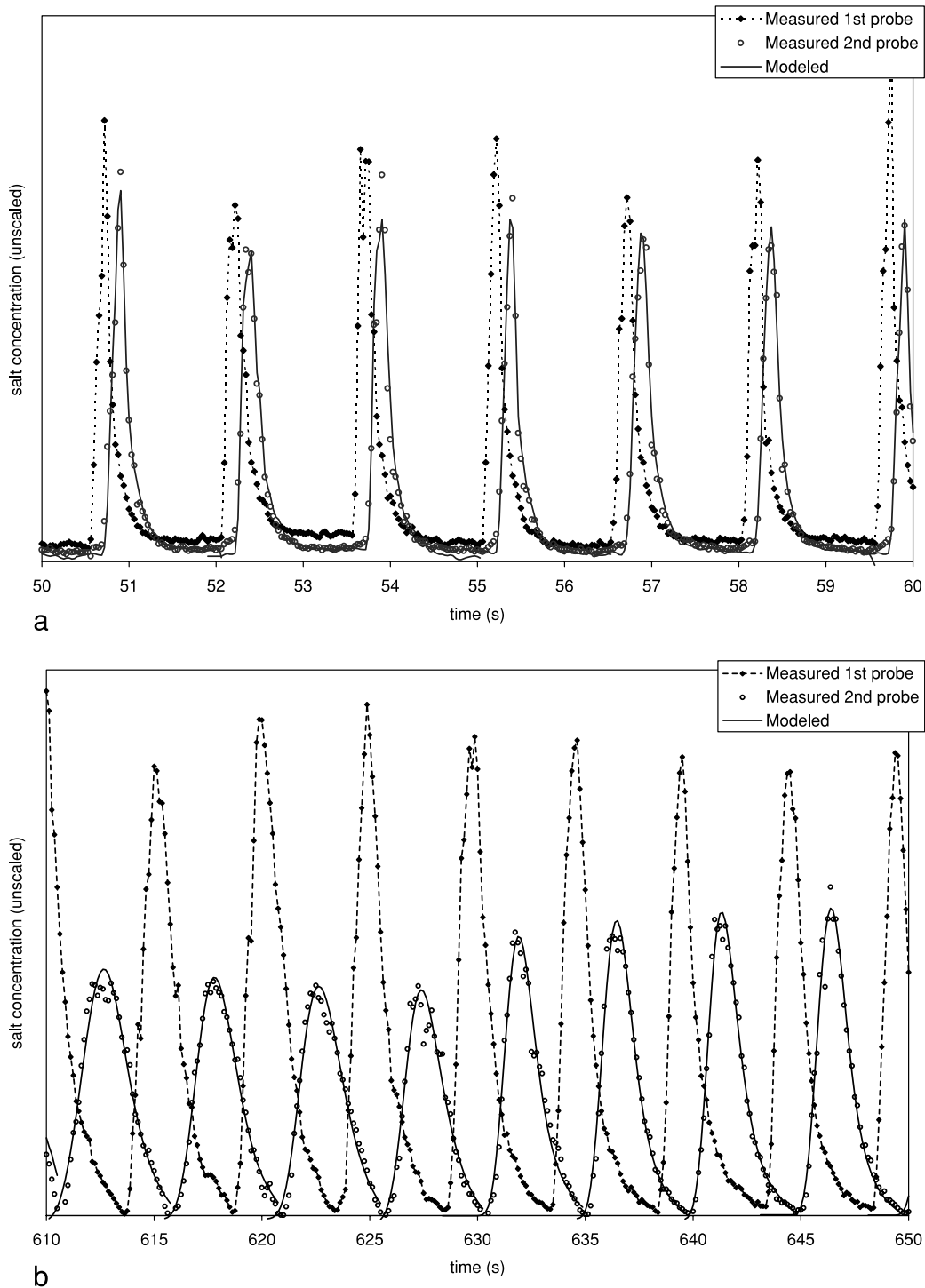


Figure 5. Modelling of peak concentrations. Dotted–dashed lines are the measured salt concentrations at the upstream probe used as model inputs. Model outputs are the salt concentrations at the downstream probe: measured (white dots) and modelled (fine solid lines). Model outputs are discontinuous since each peak is modelled independently. (a) shows the rill case and (b) the inter-rill case.

inaccuracies in the measurement itself, and inaccuracy (or bias) in the model calibration due to model incompleteness (e.g. resulting from complex diffusion processes not caught by the equation). At each of the 38 measuring points, the standard deviations of t_p and V_{Salt} were calculated from the 80 replications. The accuracy of t_p depends on the flow conditions. In the steps along the rill, where flow conditions are steady, the standard deviation of t_p ranges from 7 to 10 ms (median 9.2 ms), leading the standard deviation of V_{Salt} to range from 0.025 to 0.07 m s^{-1} (median 0.034 m s^{-1}). In the pools, where impinging flow created complex and unsteady flow fields with back-eddy re-circulation, the standard deviation of t_p ranged from 10 to 40 ms (median 19.7 ms), leading the standard deviation of V_{Salt} to range from 0.032 to 0.145 m s^{-1} .

Thus, in steady flow conditions, t_p was known with an accuracy of less than one-third of the datalogger time step (which was 31.25 ms). When the flow field was complex and unsteady, flow velocity was more variable by nature. Obtaining a mean value required the averaging of many replications. This approach was feasible however, thanks to the high sampling rate (measurements were taken at every two seconds) and the automated nature of the measuring process.

The diffusion coefficient D was not modelled with the same accuracy as t_p . The standard deviation of D roughly equals its mean value whatever the flow condition.

The inter-rill case In the inter-rill experiment, flow velocity increased rapidly up to 0.2 m s^{-1} after run-off began, and then gradually increased in an irregular manner to a maximum of 0.25 m s^{-1} . The difference between two consecutive measurements was analysed in order to evaluate the accuracy of the velocity estimates. The result showed that the standard deviation of the time to peak concentration t_p was 58.5 ms, which was approximately half the datalogger time step during this experiment (125 ms). This resulted in an accuracy of $\pm 0.006 \text{ m s}^{-1}$ for measurement of V_{Salt} .

Both experiments provided estimates of the time to peak concentration t_p with a standard error of one-third to one-half of the datalogger time step. The accuracy of the velocity differed in the two experiments according to the differences in datalogger time step, flow velocity and probe geometry.

Validation

Validation of calculated velocities was carried out in the rill-flow case. Velocity was taken at every 5 cm with the SVG with probes at 10 cm apart. Additionally, another SVG was used, with probes spaced at 34 cm to each other. This larger spacing between probes allowed the latter to take the mean velocity over the entire control section. Additionally, the mean velocity was calculated independently by dividing the known discharge (1 l s^{-1}) by the wetted area, as deduced from the cross section calculated from the DEM (2 mm resolution) and the water depth measured at every centimetre along the channel centre. Two ADV longitudinal profiles were taken in the control section, one at the water surface and one at the channel bottom, the ADV head being centred at the channel axis in both cases. In each profile, velocity measurements were spaced at one centimetre intervals. Figure 6 brings together all of these results. ADV point data are shown as squares (water surface) and triangles (rill bottom). Solid lines represent means calculated over 10 cm in order to be comparable to the results from the 10 cm salt gauge.

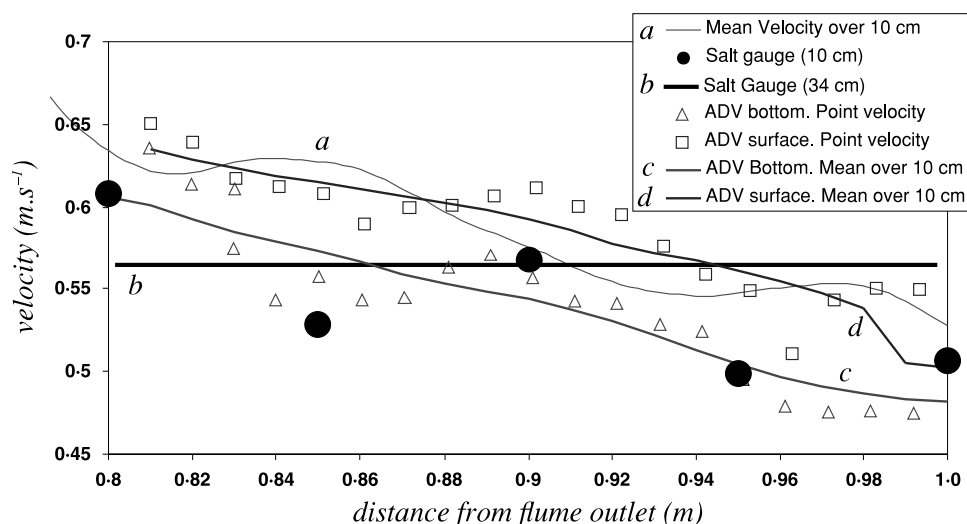


Figure 6. Velocities in the control section. Comparison of results from ADV, 10 cm SVG, 34 cm SVG and mean velocity determined directly from the continuity principle.

Table I. Mean velocities in the control section in the rill experiment derived by various methods. Comparisons, in per cent, are made with the ADV velocity (mean of surface and bottom ADV velocities)

Source	Velocity (m s^{-1})	Ratio to mean ADV (%)
ADV bottom	0.537	95.5
ADV top	0.587	95.9
ADV mean	0.562	100
10 cm salt	0.539	100.5
34 cm salt	0.565	104.5
Discharge/area	0.585	104.2

Figure 6 shows that all measurements are consistent: Table I shows that, when mean ADV results are taken as a reference, all other results are within ± 5 per cent. ADV data were preferred to the mean velocity as a reference because firstly measurements were taken at the centre of the channel, as were salt tracings, and secondly, because of turbulence, the water surface is not flat or smooth, which can lead to a biased measurement of flow depth.

In Figure 6 as in Table I, results from the 10 cm salt gauge appear closer to the bottom velocity than to the top velocity. The higher density of the salt solution, which causes it to sink, could explain this pattern.

Discussion

The approach presented here differs from the classical use of tracers in flow velocity measurement. The most important differences are the following.

- All data collected contribute to the model results, and not only the time to peak concentration or the leading-edge time.
- The mean velocity of the plume is directly estimated. The need for a correcting factor α is consequently avoided.

These choices have led to an unbiased measurement of the mean velocity of the tracer, as shown in Figure 6 and Table I.

Two questions can now be discussed.

- Which part of the flow is measured by this technique?
- What can be learned from these equations on the known variability of the ratio of the leading-edge velocity to mean flow velocity (α) and the ratio of peak velocity to mean flow velocity (β)?

Field significance of calibrated velocities

The preceding sections have shown that the entire salt plume was correctly modelled, which gave us confidence that the calibrated velocity was the mean velocity of the tracer. However, it is clear that the measured velocity is no longer the mean velocity of the flow, but only the mean velocity of the traced flow threads. Thanks to the small length of the control section, the lateral location and extent of the plume can be known. Adding potassium permanganate to the salt solution is a way of visualizing the lateral extent of the plume. However, it is unfortunately not possible to determine the vertical distribution of the tracer. In this experiment, saturated brine was used in order to maximize the peak quality. This approach may have led to a poor mixing of the tracer and the flow. Further improvements the SVG technology will have to tackle the mixing of the tracer and the flow. Reducing the volume of tracer to a single brine droplet could enable us to measure the velocity of a single flow thread. Conversely, increasing the distance between injection and the first probe could lead to get closer to the measurement of V_{mean} .

Variability of α and β

Values of α have been calculated numerically and β is derived from Equation 4 for the observed ranges of C and D obtained during the experiments. Values of x were taken within the range of 0.5–2 m, which is a commonly used control section length for dye tracing.

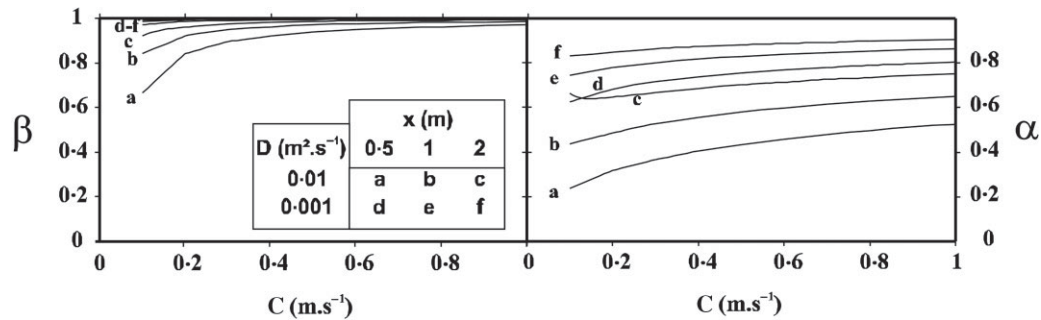


Figure 7. Correction factors α and β predicted by the 1D diffusion wave equation with common values of control section length x and diffusion coefficient D (curves a to f), and velocity V (abscissa).

Figure 7 shows how much α , and to a lesser extent β , can vary with the length of the control section and, moreover, with diffusion. It is acknowledged that Figure 7 was derived from extrapolations of limited experimental results from the observed range of x values. However, there is some evidence that the diffusive effects observed on short lengths in the experiment will not disappear in larger control sections but, on the contrary, will contribute to other diffusion effects caused by the more complex behaviour of the tracer plume along longer sections. As a consequence, values of α and β in Figure 7 should be considered as upper boundaries. As an example, the experiment of Li *et al.* (1996), with a control section of 2.6 m long and mean velocities in the range of 0.2–0.5 m s⁻¹ (mean 0.3 m s⁻¹), yielded values of α in the range 0.4–0.7 (mean 0.5), and of β in the range of 0.6–0.9 (mean 0.8). These values are significantly lower than those predicted by Figure 7.

At this point of the discussion, it can be concluded that the diffusion-wave equation has proved its efficiency in modelling the behaviour of a tracer plume over a short distance. This equation shows that the correction factors α and β are not constant but depend on V , D and x . Numerical experiments have shown that these variations may explain, at least partially, the variations of α and, to a lesser extent, β cited in the literature.

This result is consistent with the scattering of α values mentioned by Dunkerley (2001). His conclusion – that it is not possible to estimate reliably the mean velocity from the timing of the leading edge of a tracer plume – is strengthened.

Probe design

The SVG technology is intrusive: probes must be in contact with the flow. Special attention must therefore be paid to the probe design in order to combine good peak detection and low impact on erosion and deposition processes. The horizontal probes of Figure 1 proved very sensitive but have caused serious additional deposition. The vertical design of Figure 4 was accurate enough regarding peak quality and did not cause any sediment deposit. Scouring occurred however when the flow was supercritical (Froude number > 1).

Probe spacing is another concern. Additional experiments (to be detailed in a separate paper) have shown that while fast turbulent flow may accommodate probe distance as short as 3 cm (providing the datalogger is fast enough), slow laminar flow may not work properly when the probe distance is less than 10 cm. Adding potassium permanganate to the salty water was found to be very useful when setting up a specific experimental protocol.

Conclusion

This paper has shown an enhancement of the classical salt-tracing technique for measuring flow velocity. Enhancements have been made in four ways.

- By measuring velocity between two probes rather than between the injection point and a probe, it is possible to avoid having to take into account the unpredictable behaviour of the salt solution hitting the flow surface and diffusing intensively while accelerating.
- Shortening the length of the control section. Inter-probe distances of 10 cm and 40 cm were used, allowing a 1D model to fit the observed data.
- Automating the salt injection in order to generate a salt plume at 2–10 s intervals, depending on the expected velocity and distance between probes. Increasing the frequency of injections offsets the precision losses due to short control sections.

- Modelling each salt plume separately with a 1D diffusion model, using the analytical solution of Hayami (1951) to the 1D diffusion-wave equation. Compared with the traditional timing of either the peak or the leading edge, modelling the entire plume yields three main results. First, the calibrated times are no longer multiples of the datalogger time step, but vary continuously. Second, all the available information is involved in the computation, resulting in a significant enhancement of the resolution. Consequently, the resolution of peak time was one-third to one-half of the datalogger time step. Third, since the 1D model produces coefficients of determination ≥ 90 per cent, the model outputs the true mean velocity of the salt plume. This result does not need any additional correction factor.

Tested flow velocities ranged from 0.05 to 0.7 m s⁻¹ when measured in the rill experiment and from 0.02 to 0.3 m s⁻¹ in the interrill experiment. Resolution of the measurement was governed by the precision of the modelling of the peak time. In the best flow conditions, peak time was known with a precision of one-third of the datalogger time step, leading to a resolution of the flow velocity between 0.006 and 0.034 m s⁻¹, depending on the distance between probes and the datalogger time step. Increasing the sampling rates would probably yield better precision in those cases.

In the rill case, SVG velocities agreed with ADV measurements. It is therefore concluded that the SVG technology, which combines a new salt gauge and a dedicated numerical model, provides unbiased measurement of the mean velocity of the traced plume.

However, the knowledge of the precise location of the flow thread followed by the salt plume remains vague, particularly in the vertical dimension. The salt is neither homogeneously distributed vertically nor specifically located at the flow bottom, despite being denser than pure water. More field experience of this technology and additional validation by independent velocity measurements should enlighten this point.

Further developments of the technique could go in the following directions:

- use a device capable of a higher recording rate;
- use brine droplets instead of continuous jets;
- miniaturize the salt gauge;
- run the model in real time;
- better control of the mixing of the tracer and the flow.

Notation

A	Wetted area (m ²)
Q	Flow discharge (m ³ s ⁻¹)
V_{Salt}	Mean flow velocity within the plume (m s ⁻¹)
V_{Max}	Maximum flow velocity within the plume (m s ⁻¹)
V_{Mean}	Mean flow velocity (m s ⁻¹)
D	Diffusion coefficient (m ² s ⁻¹)
d	Distance between probes (m)
x	Distance along the flow (m)
$C_1(t)$	Relative salt concentration at the first probe ($x = 0$) and time t (g l ⁻¹)
$C_2(t)$	Relative salt concentration at the second probe ($x = d$) and time t (g l ⁻¹)
$C(x, t)$	Hayami's equation at time t and location x (g l ⁻¹)
Δt	Time step of the measured data (s)
α	Ratio of leading-edge velocity to mean flow velocity (dimensionless)
β	Ratio of peak velocity to mean flow velocity (dimensionless)
t_p	Time (s) of peak salt concentration at the second probe ($x = d$). Peak time is the abscissa of the maximum of function $C(x, t)$ (Equation 3).

References

- Acton FS. 1970. *Numerical Methods that Work*, corrected edition 1990. Mathematical Association of America, Washington; 464–467.
- Adrian RJ. 1991. Particle-imaging techniques for experimental fluid mechanics. *Annual Review of Fluid Mechanics* **23**: 261–304.
- Ayala JE, Martínez-Austria P, Menéndez JR, Segura FA. 2000. Fixed bed forms laboratory channel flow analysis. *Ingeniería Hidráulica En México* **15** (2): 75–84.

- Dunkerley DL. 2001. Estimating the mean speed of laminar overland flow using dye injection-uncertainty on rough surfaces. *Earth Surface Processes and Landforms* **26**: 363–374.
- Dunkerley DL. 2003. An optical tachometer for short-path measurement of flow speed in shallow overland flows: improved alternative to dye timing. *Earth Surface Processes and Landforms* **28**: 777–786.
- Emmett WW. 1970. *The Hydraulics of Overland Flow on Hillslopes*, Professional Paper 662-A. United States Geological Survey; Washington, DC.
- Favis-Mortlock DT, Boardman J, Parsons AJ, Lascelles B. 2000. Emergence and erosion: a model for rill initiation and development. *Hydrological Processes* **14**: 2173–2205.
- Gimenez R, Planchon O, Silvera N, Govers G. 2004. Longitudinal velocity patterns and bed morphology interaction in a rill. *Earth Surface Processes and Landforms* **29**: 105–114.
- Hayami S. 1951. *On the Propagation of Flood Waves*, Bulletin No. 1. Disaster Prevention Research Institute, Kyoto University.
- Henderson FM. 1966. *Open Channel Flow*. New York: Macmillan.
- Horton RE, Leach HR, Van Vliet R. 1934. Laminar sheet-flow. *Transactions of the American Geophysical Union* **15**: 393–404.
- Li G, Abrahams AD. 1997. Effect of saltating sediment load on the determination of the mean velocity of overland flow. *Water Resources Research* **33**: 341–347.
- Li G, Abrahams AD, Atkinson JE. 1996. Correction factors in the determination of mean velocity of overland flow. *Earth Surface Processes and Landforms* **21**: 509–515.
- Liu Z, Adrian RJ, Hanratty TJ. 2001. Large-scale modes of turbulent channel flow: transport and structure. *Journal of Fluid Mechanics* **448**: 53–80.
- Myers TG. 2002. Modelling laminar sheet flow over rough surfaces. *Water Resources Research* **38** (11), 1230. DOI: 10.1029/2000WR000154.
- Planchon O, Cadet P, Lapetite JM, Silvera N, Esteves M. 2000a. Relationship between raindrop erosion and runoff erosion under simulated rainfall in the Sudano-Sahel. Consequences for the spread of nematodes by runoff. *Earth Surface Processes and Landforms* **25** (7): 729–741.
- Planchon O, Esteves M, Silvera N, Lapetite JM. 2000b. Raindrop erosion of tillage induced microrelief. Possible use of the diffusion equation. *Soil and Tillage Research*. **56** (3/4): 131–144.
- Press WH, Teukolsky SA, Vetterling WT, Flannery BP. 1992. *Numerical Recipes in C. The Art of Scientific Computing*, 2nd edn. Cambridge University Press: Cambridge.
- Quinn P, Beven K, Chevallier P, Planchon O. 1991. The prediction of hillslope flow paths for distributed hydrological modelling using digital terrain models. *Hydrological Processes* **5** (59): 59–79.
- Raffel M, Willert C, Kompenhans J. 1998. *Particle Image Velocimetry, a Practical Guide (Experimental Fluid Mechanics)*. Springer: Berlin.
- Robinson KM, Cook KR. 1998. Stress measurement upstream of an overfall. *Transactions of the ASAE* **41** (4): 1019–1024.
- Takken I. 2000. *Effects of Roughness on Overland Flow and Erosion*. PhD Thesis. Katholieke Universiteit Leuven.